https://dx.doi.org/10.22161/ijaers.69.12 *ISSN: 2349-6495(P) | 2456-1908(O)*

Preparation, Structural and Magnetic Characterization of the $BaTi_{(1-x)}Mn_xO_3$ System

Larissa Galante Dias[1], Marcelo Rodrigo Munhoz[1], Leandro Bertaco Lucio[1], Gustavo José Correa Gonçalves[1], Ricardo Breganon[2], Fernando Sabino Fonteque Ribeiro[2], Ricardo Augusto Mascarello Gotardo[3]

[1]Faculdade Estácio de Sá de Ourinhos, OURINHOS, SÃO PAULO, BRAZIL
Email: larissa.dias@estacio.br; marcelo.munhoz@estacio.br; leandrobertaco@live.com; gustavo.correa@estacio.com
[2]Federal Institute of Paraná, JACAREZINHO, PARANÁ, BRAZIL
Email: ricardo.breganon@ifpr.edu.br; fernando.ribeiro@ifpr.edu.br
[3]Federal Technologic University of Paraná, MEDIANEIRA, PARANÁ, BRAZIL
Email: rgotardo@utfpr.edu.br

Abstract*—The $BaTiO_3$ is one of the most studied ferroelectric materials mostly due to its great potential for technological applications. Recently, other properties have been explored in $BaTiO_3$, such as photoluminescence, photoacoustic and magnetism. These characteristics are mainly found when replacing the Ba and Ti ions by other transition metals or rare earths ions. The solid state reaction technique was used to prepare solid solutions of $BaTi_{(1-x)}Mn_xO_3$, in which the precursors $BaCO_3$, TiO_2 e MnO_2 were weighed according to desired stoichiometry, for x between ($0.001 \leq x \leq 0.1$) and placed in the mill for 24 hours. Then, the obtained solid solution was calcined at a temperature of 1200 ° C for 1 hour. After calcination, the solid solution $BaTi_{(1-x)}Mn_xO_3$, were analyzed by X-ray diffraction, scanning electron microscope and by a magnetometer vibrating sample to verify the existence of magnetic properties. The results presented in this work are satisfactory, where we obtained a multiferroic material.*

Keywords*—*$BaTiO_3$, Multiferroics, Magnetic Properties.

I. INTRODUCTION

The study and development of new materials are extremely important for the discovery of new technologies. Material science is directly linked to technological advances, and the manufacturing process is a determining factor for the properties of materials. Different manufacturing methods lead to different structural and microstructural properties, which are directly linked with mechanical, thermal, electrical and magnetic properties.

An example of material with great technological application is barium titanate, $BaTiO_3$. A ceramic material whose main property is ferroelectricity [1]. The $BaTiO_3$ was one of the first discovered materials to have a perovskite structure and has five solid state phases with symmetries: hexagonal, cubic, tetragonal, orthorhombic and rhombohedral, which have ferroelectricity, except for the cubic phase [2, 3]. Another characteristic of $BaTiO_3$ are the piezoelectricity and the high dielectric constant values, that are between 1500 and 2000 [4, 5], therefore, it can be used, for example, in capacitors, high voltage insulators, transducers, microphones and electro-optical devices [1,6]. Recently some other properties have been explored in the $BaTiO_3$, such as photoluminescence, photoacoustics and magnetism, these characteristics are mainly found when replacing Ba and Ti ions with other transition metals or rare earth ions.

The method generally used to obtain the $BaTiO_3$ is the solid state reaction, using as precursors $BaCO_3$ and TiO_2, this process is realized at temperatures higher than 1000 ºC [7]. The resulting grains of this synthesis method are not uniform and have an average size higher than 1 μm [8]. Impurities such as Barium Carbonate ($BaCO_3$) and other unwanted phases may appear during material synthesis [7]. Other methods of preparing the $BaTiO_3$ are high energy milling, sol-gel, hydrothermal synthesis and pechini [1, 9, 10]. The synthesis method directly influences the final properties of the material. Substitution is one of the forms to modify the microstructure, structure and other ceramic properties of $BaTiO_3$ [1]. These substitutions are determining factors for the applications of these ceramics and can be applied as high voltage insulators, semiconductors, ferroelectrics usable in the manufacture of capacitors and memories for computers [11]. In order to improve the electrical properties of the $BaTiO_3$, Ba and Ti

https://dx.doi.org/10.22161/ijaers.69.12 *ISSN: 2349-6495(P) | 2456-1908(O)*

ions are replaced by other elements such as Mn (manganese) for example, substitutions may be made in the material in the form of ceramic or in the form of thin film [12]. Another dominant characteristic regarding substitution for $BaTiO_3$, with the Mn ion is to make it a promising candidate when aiming for magnetic properties after substitution [13].

Presenting magnetic and ferroelectric properties after Mn substitution, the material can be classified as multiferroic and can present magnetoelectric effects, that is, appearance of a magnetization due to an electric field or appearance of an electrical polarization due to a magnetic field. This effect makes multiferroic materials extremely interesting for applications where the same material needs to perform more than one task and with that a crescent interest has been devoted to them. It has also been reported that double substitution by two transition metal ions, Fe and Mn for example, makes $BaTiO_3$ present excellent magnetic properties[13].

Thus, this work proposes to synthesize through the method of synthesis of the post-ceramic solid state of $BaTiO_3$ substitute Ti ions with Mn ions, forming the compound $BaTi_{(1-x)}Mn_{(x)}O_3$, which $0.001 \leq x \leq 0.1$. The objective is to obtain a material that presents in the same phase ferroelectricity and (anti)ferromagnetism and to study the effects of the substitution of Ti by the ions of Mn in the structural, microstructural and magnetic properties.

II. MATERIALS AND METHODS

Through the solid state reaction synthesis method, the solid solution was obtained $BaTi_{(1-x)}Mn_xO_3$, using the precursors $BaCO_3$, TiO_2 e MnO_2 with analytical purity.

The stoichiometric calculations through the molar masses of the compounds were performed and it was possible to verify the necessary masses of each precursor to produce 15 grams of $BaTi_{(1-x)}Mn_xO_3$, where the values are presented in Table 1, concentration varied in compositions between $0.001 \leq x \leq 0.1$, which were used for the stoichiometric calculations.

Table 1- Precursor masses for 15 grams of $BaTi_{(1-x)}Mn_xO_3$ calculated stoichiometrically

	PRECURSOR	MOLAR MASS	MASS (g)
Substitution (X=0.001)	$BaC0_3$	197.335	10.7058
	TiO_2	79.865	4.2895
	MnO_2	86.936	0.0047
Substitution (X=0.01)	$BaC0_3$	197.335	10.6756
	TiO_2	79.865	4.2774
	MnO_2	86.936	0.0470
Substitution (X=0.03)	$BaC0_3$	197.335	10.6701
	TiO_2	79.865	4.1888
	MnO_2	86.936	0.1410
Substitution (X=0.05)	$BaC0_3$	197.335	10.6647
	TiO_2	79.865	4.1004
	MnO_2	86.936	0.2349
Substitution (X=0.1)	$BaC0_3$	197.335	10.6511
	TiO_2	79.865	3.8796
	MnO_2	86.936	0.4692

After the calculations were performed, the compounds were weighed on an analytical balance with a tolerance of ± 0.0001g and mixed in a container. Then the materials ware mixed with distilled water and 10 mm diameter zirconium spheres, in order to fill the container volume. The container was sealed and taken to the mill where it rotated for 24 hours for the purpose of mixing the precursors. The mixture was then separated from the spheres and put in the microwave oven for periods ranging from 30 to 35 minutes, enough to dry the distilled water of the composition.

After the drying process, the material passed by thermic treatment (calcination) the temperature used was 1200ºC and the time was 1 hour for all compositions. X-ray diffraction was realized, data were obtained by means of an X-ray diffractometer with radiation CuKα with λ=1.5418 Å. The electrical voltage in the tube was 40kV, the electric current was 30mA and the scan mode used was fixed time, with a range of 20° to 80°, 0.02 step and 8 second time.

The diffractogram peaks were indexed with records from the international database JCPDS (Joint Committee for Powder Diffraction Studies). After the samples were finalized, observations were made in a scanning electron microscope model JEOL SM 5800 LV with orders of magnitude from about 5000 to 10000 times.

The determination of the magnetic hysteresis curve was obtained by a homemade the vibrating sample magnetometer, where the samples were submitted to vibration with the presence of a magnetic field, using a magnetometer to evaluate the magnetic field produced. Finally, using the unit cell volume obtained by X-ray diffraction and the unit cell mass, the theoretical density of the materials was calculated. Theoretic density is indicated by Equation 1, where m_c is the unit cell mass and V_c the unit cell volume.

$$\rho_{\text{theoretic}} = \frac{m_c}{V_c} \quad (1)$$

The unit cell volume in the tetragonal phase is calculated by Equation 2, where a, b and c are the lattice parameters of the cell. For the hexagonal symmetry unit cell, its volume is given by Equation 3. For both conditions, a=b≠c [16].

$$V_{ct} = a^2 . c \quad (2)$$

https://dx.doi.org/10.22161/ijaers.69.12 *ISSN: 2349-6495(P) | 2456-1908(O)*

$$V_{ch} = \frac{6a^2\sqrt{3}}{4}.a \quad (3)$$

The lattice parameters are obtained by the relation, for tetragonal symmetry, between the Miller indices and the interplanar distance d_{hkl}, presented in Equation 4 [14]. For the hexagonal phase the lattice parameters were obtained through Equation 5. The interplanar distance d_{hkl} can be obtained by applying Equation 6. For the calculation of the unit cell mass, the sum of the product of the atomic masses by the contributing atoms in the unit cell. Atomic mass can be calculated by Equation 7.

$$\frac{1}{d_{hkl}^2} = \frac{h^2+k^2}{a^2} + \frac{l^2}{c^2} \quad (4)$$

$$\frac{1}{d_{hkl}^2} = \frac{4}{3}\frac{h^2+h.k+k^2}{a^2} + \frac{l^2}{c^2} \quad (5)$$

$$d_{hkl} = \frac{n\lambda}{2\ \mathrm{Lsin}\,\theta} \quad (6)$$

$$m_{atomic} = \frac{m_{molar}}{N_A} \quad (7)$$

III. EXPERIMENTAL RESULTS

To discuss the results, this work was divided into: scanning electron microscopy (SEM) analysis, phase analysis of $BaTi_{(1-x)}Mn_xO_3$, tolerance factor, lattice parameters, density and magnetic hysteresis [17].

The Figures 1, 2, 3 and 4 show the SEM images. Figures 1 and 3 present the micrographs of the samples of pure $BaTiO_3$, while Figures 2 and 4 show the micrographs of the material $BaT_{(1-x)}Mn_xO_3$ with different substitution concentrations.

In the scanning electron microscopy analysis, a comparison was made between the pure $BaTiO_3$ and for the substitution concentrations of x=0.01 (Figure 2(a) and Figure 4(a)), it was found that the grains began to suffer a bonding between them but there was no change when compared the grain sizes.

In the sample analysis for x = 0.03 (Figures 2(b) and 4(b)) a larger bonding was found when compared to the composition with x = 0.01, and some grains started to reduce in size. For the concentration of x=0.05 as illustrated in the Figures 2(c) and 4(c), it was possible to identify a larger quantity of particles assuming smaller sizes and a bonding between them larger than those presented by the samples of smaller concentrations of Mn. Figures 2(d) and 4(d) shows the micrographs of the samples with x=0.1, in which it is possible to observe more accurately the reduction in the grain sizes and the manifestation of grains in rectangular forms. In this sample the bonding between them becomes even larger, certifying that with increasing concentration, the grains join significantly.

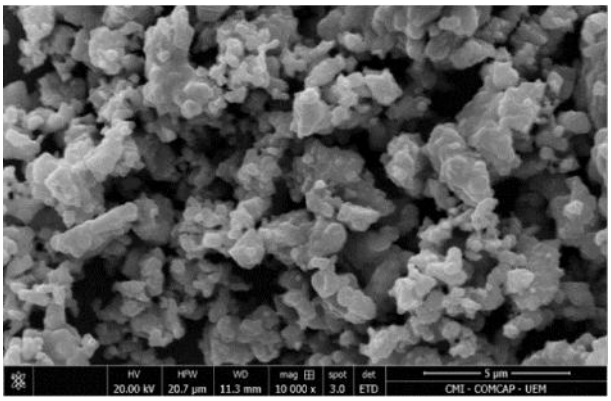

Fig. 1: Micrograph sample of $BaTi_{(1-x)}Mn_{(x)}O_3$ for x = 0

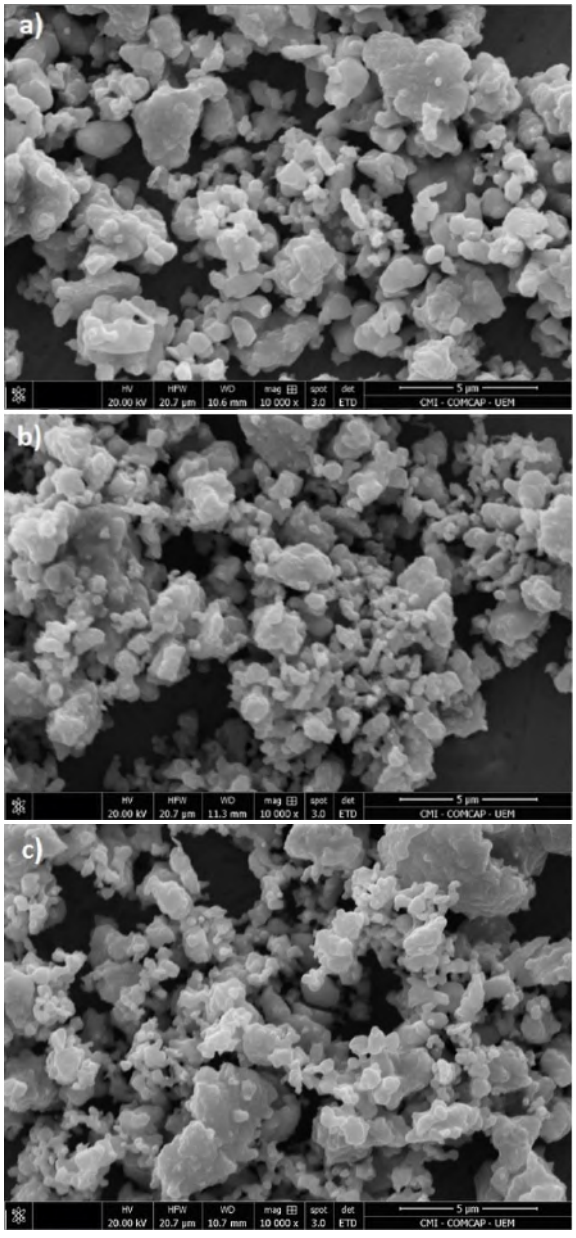

https://dx.doi.org/10.22161/ijaers.69.12 *ISSN: 2349-6495(P) | 2456-1908(O)*

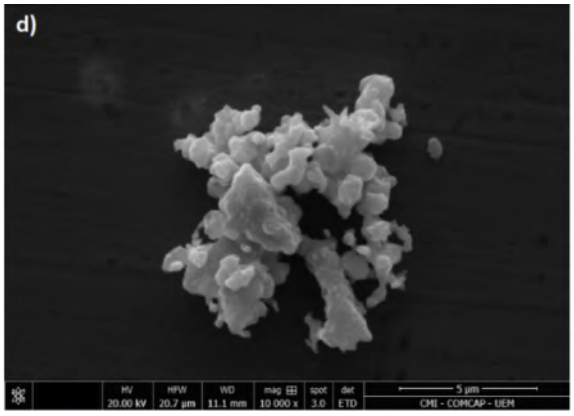

Fig. 2: Microstructural analysis of samples (a)$BaTi_{(1-x)}Mn_{(x)}O_3$ (x=0.01) (b) $BaTi_{(1-x)}Mn_{(x)}O_3$ (x=0.03) (c) $BaTi_{(1-x)}Mn_{(x)}O_3$ (x=0.05) (d) $BaTi_{(1-x)}Mn_{(x)}O_3$ (x=0.1)

Through the micrographs analysis it was possible to verify that the changes in the grains occur due to the substitution of the Ti ions by Mn in $BaTiO_3$, generating a reduction in grain size and when examined in relation to its distribution, it was found that there was a significant bonding between them.

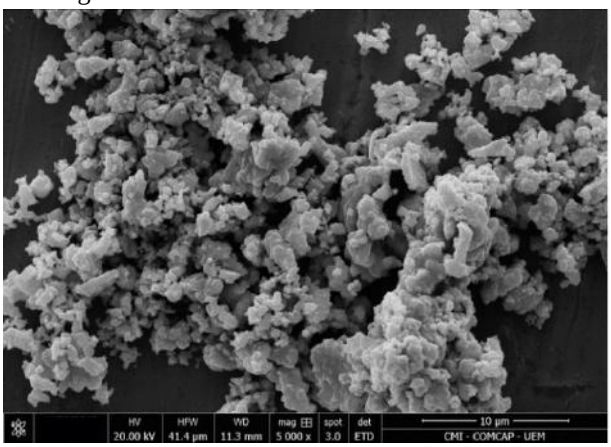

Fig. 3: Micrograph sample of $BaTi_{(1-x)}Mn_{(x)}O_3$ for x = 0

The phase analyzes of the of $BaTi_{(1-x)}Mn_xO_3$ samples were performed using the x-ray diffractometer, for the purpose of checking the purity of the material. Figure5 shows the diffractogram patterns of pure$BaTiO_3$ in a temperature range from 950ºC to 1200ºC. When calcined at a temperature of 950ºC a second phase can be observed, which for this case is $BaCO_3$, the peaks were identified with (●).

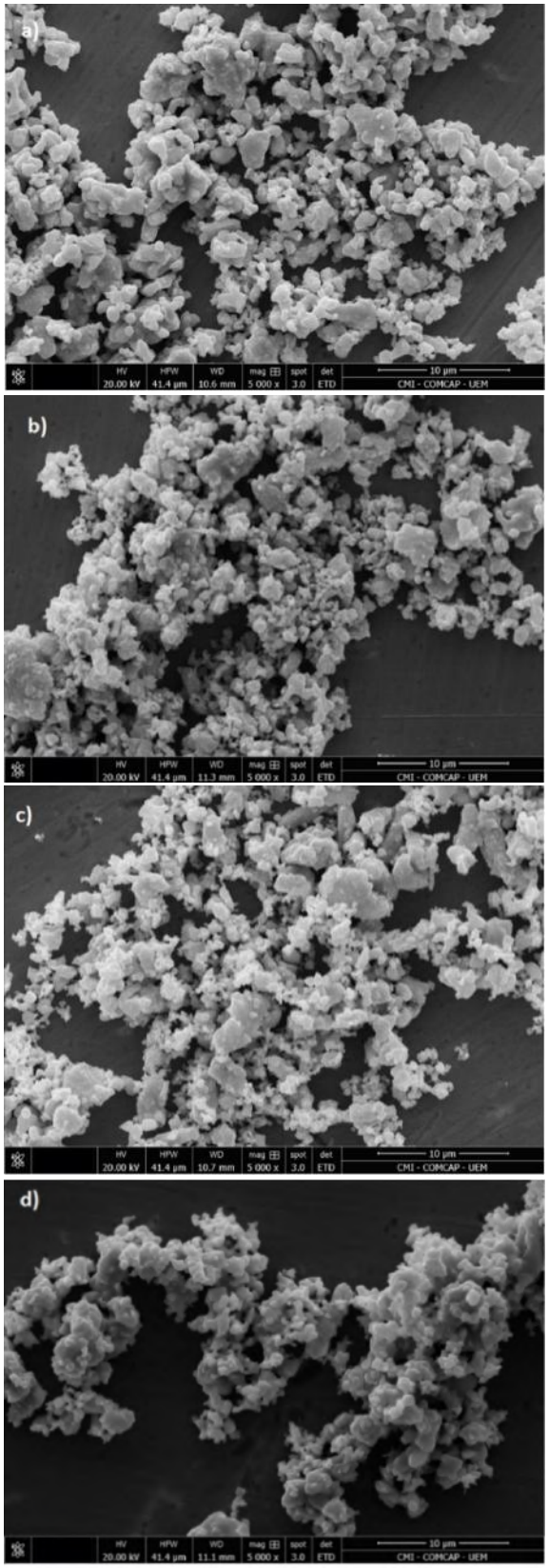

Fig. 4: Microstructural analysis of samples (a)$BaTi_{(1-x)}Mn_{(x)}O_3$ (x=0.01) (b) $BaTi_{(1-x)}Mn_{(x)}O_3$ (x=0.03) (c) $BaTi_{(1-x)}Mn_{(x)}O_3$ (x=0.05) (d) $BaTi_{(1-x)}Mn_{(x)}O_3$ (x=0.1).

https://dx.doi.org/10.22161/ijaers.69.12 *ISSN: 2349-6495(P) | 2456-1908(O)*

For pure $BaTiO_3$ calcined at 1000ºC, is the same situation where $BaCO_3$ is present as a secondary phase, but less evident. Already for pure $BaTiO_3$ calcined at 1100 ºC, $BaCO_3$ is present in a small amount, but a Ba_2TiO_4 phase is formed, marked with asterisk (*) in Figure 5. In the case of the pure $BaTiO_3$ calcined at 1150 ºC, the $BaCO_3$quantity seems is lower than the sample calcined at 1100ºC, but with a higher amount of Ba_2TiO_4, as shown in Figure 5.

And finally, the diffractogram of $BaTiO_3$solid solution calcined at 1200 ºC, presented the most satisfactory result, because when calcined at this temperature occurs the elimination of the $BaCO_3$ phase, leaving only the Ba_2TiO_4 phase, and thus presenting a smaller amount of impurities.

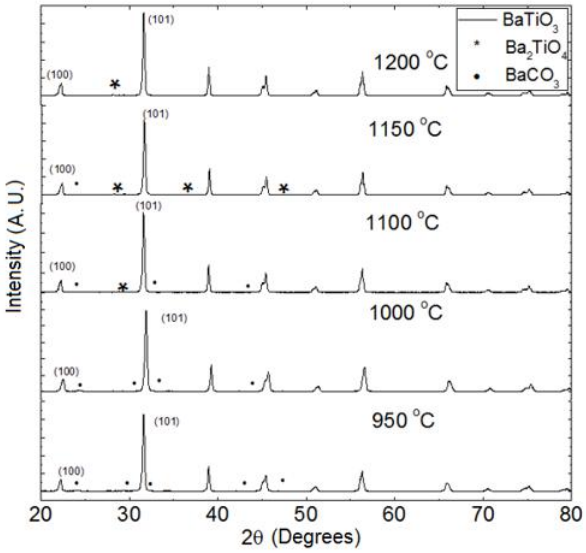

Fig. 5: Difratogram of $BaTiO_3$ calcined – Temperature between 950ºC and 1200ºC

Through X-ray diffraction insolid solution of $BaTi_{(1-x)}Mn_xO_3$ it was possible to verify the purity of the material and to identify the phases of the same, the diffractograms are presented in Figures 6, 7, 8, 9 and 10. Figure 6 is the diffractogram of $BaTi_{(1-x)}Mn_xO_3$ sample calcinated at 1200 ºC, with concentration of x=0.001, in which a second phase can be observed, which for this case is $BaCO_3$. Through data sheets JCPDS 75-1606 and 01-0506it was possible to obtain the symmetry of the material ($BaTi_{(1-x)}Mn_xO_3$), with tetragonal characteristics.

Figure 7 shows the diffractogram of $BaTi_{(1-x)}Mn_xO_3$ sample calcined at 1200ºC, with concentration of x=0.01, in which a second phase of $BaCO_3$ is also present, at the peaks with an asterisk, according to Figure5. In this composition it is still possible to observe that for $BaTi_{(1-x)}Mn_xO_3$ there is only the tetragonal phase, the data sheets obtained to find the symmetry of the material were JCPDS 75-1606 and 01-0506.

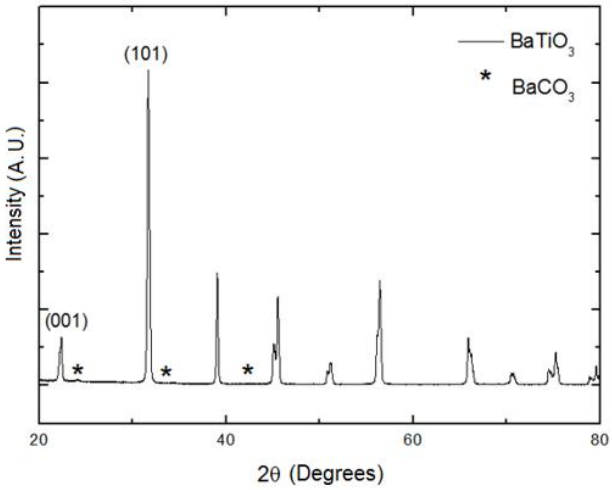

Fig. 6: Diffractogram of $BaTi_{(1-x)}Mn_xO_3$ calcined at 1200 ºC for x=0.001.

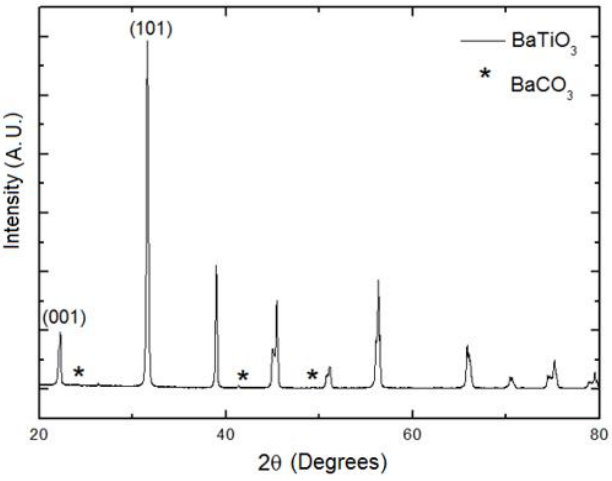

Fig. 7: Diffractogram of $BaTi_{(1-x)}Mn_xO_3$ calcined at 1200 ºC for x=0.01.

In Figure 8 with a higher substitution concentration (x=0.03) there is now hexagonal symmetry, beyond the tetragonal in the compound. Through the diffractogram it is also possible to identify the presence of the phase $BaCO_3$, the data sheets JCPDS used were 81-2201, 01-0506, 34-0129. Figure 9 with a concentration of x=0.05 the tetragonal and hexagonal symmetry remains in the compound, and it is still possible to identify the presence of $BaCO_3$ impurity.

And finally, in Figure 10, with the highest concentration of Mn (x = 0.1) it is possible to observe that the material has only hexagonal symmetry. Moreover, it presents impurity in its composition, $BaCO_3$, represented by the asterisk in the peaks.

https://dx.doi.org/10.22161/ijaers.69.12 *ISSN: 2349-6495(P) | 2456-1908(O)*

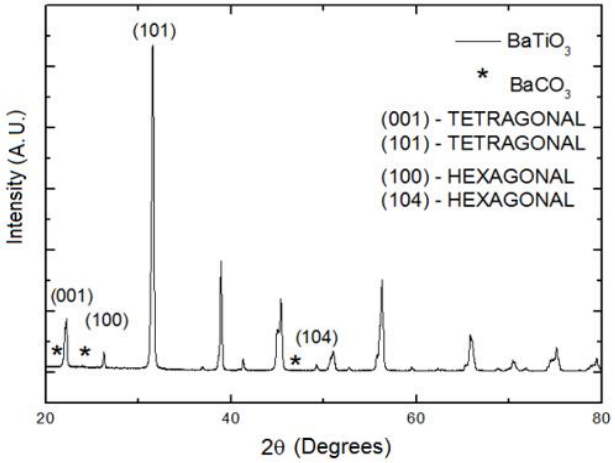

Fig. 8: Diffractogram of $BaTi_{(1-x)}Mn_xO_3$ calcined at 1200 ºC for x=0.03.

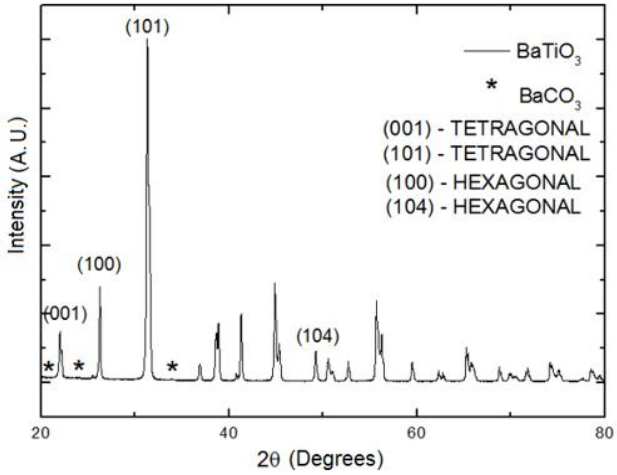

Fig. 9: Diffractogram of $BaTi_{(1-x)}Mn_xO_3$ calcined at 1200 ºC for x=0.05.

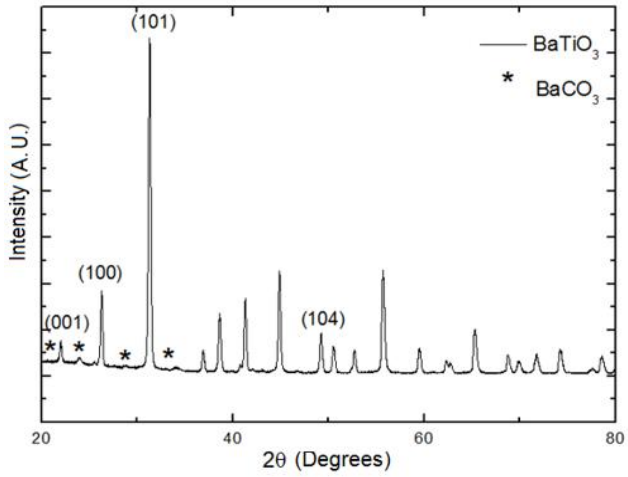

Fig. 10: Diffractogram of $BaTi_{(1-x)}Mn_xO_3$ calcined at 1200 ºC for x=0.1.

Tolerance factor analysis is given from ionic radius (Equation 8). For the structure to remain cubic, the tolerance factor must be between 0.95 < t < 1.0. Through the calculations of the tolerance factor for $BaTiO_3$ and $BaTi_{(1-x)}Mn_xO_3$ it is obtained that when the substitution of the Ti ion by Mn occurs the structure in no longer cubic, acquiring the property of ferroelectricity.

$$t = \frac{1}{\sqrt{2}} \frac{(R_A + R_O)}{(R_B + R_O)} \quad (8)$$

The ionic radius used to calculate the tolerance factor were Mn=0.067nm, 0=0.140nm, Ba=0.136nm, Ti=0.068nm [16]. For $BaTiO_3$ the tolerance factor has a value of 0.94 which is a value that is not within the range of a cubic structure, as it has a tetragonal structure.

The calculations were also performed for the compositions $BaTi_{(1-x)}Mn_xO_3$ obtaining a value of 0.94, ie, they also do not have a cubic structure having ferroelectricity.

Through the diffractograms we obtained the necessary data to find the lattice parameters "a" and "c" through Equation 4 (tetragonal symmetry) and Equation 5 (hexagonal symmetry). Figures 11 and 12 shows the lattice parameters for pure $BaTiO_3$ and $BaTi_{(1-x)}Mn_xO_3$ at a calcination temperature of 1200ºC both with tetragonal symmetry.

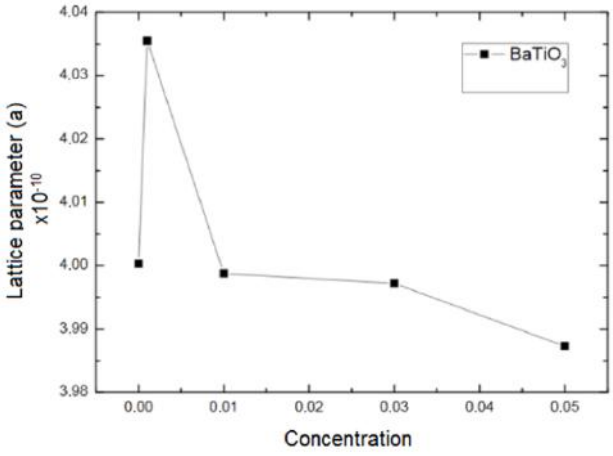

Fig. 11: Lattice Parameter "a" – Tetragonal Symmetry - calcined at 1200ºC.

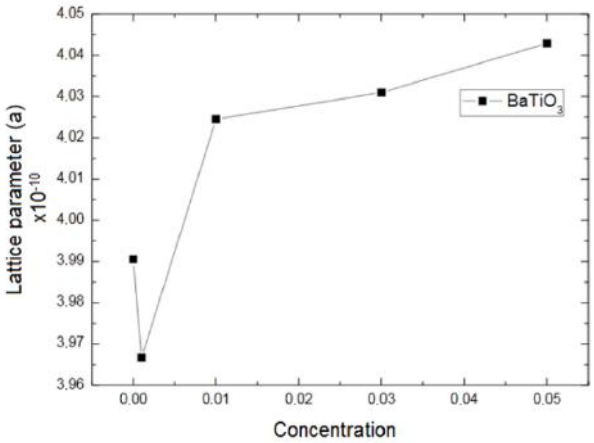

Fig. 12: Lattice Parameter "c" – Tetragonal Symmetry - calcined at 1200ºC.

https://dx.doi.org/10.22161/ijaers.69.12 *ISSN: 2349-6495(P) | 2456-1908(O)*

Through the analyzes performed on the samples it was possible to identify that the tetragonal phase was present up to a concentration of 5% Mn (x = 0.05), increasing to a 10% Mn concentration in $BaTi_{(1-x)}Mn_xO_3$ material causes the cell to stretching and tetragonal symmetry ceases to exist, and only hexagonal symmetry is present. In Figures 13 and 14 it is possible to identify that the presence of the hexagonal phase can be identified from the concentration of 3% Mn (x = 0.03), this concentration of Mn at which the cell starts to stretch.

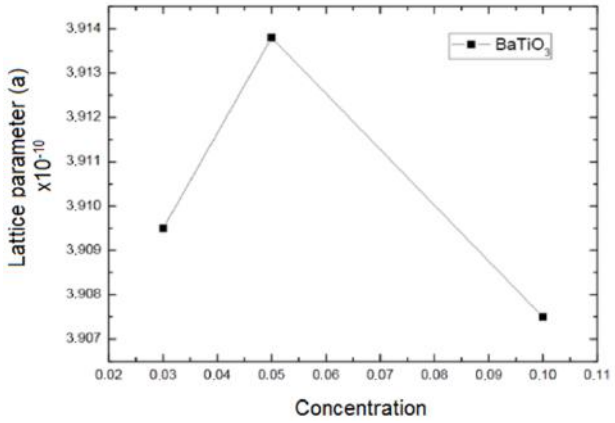

Fig. 13: Lattice Parameter "a" – Hexagonal Symmetry - calcined at 1200ºC.

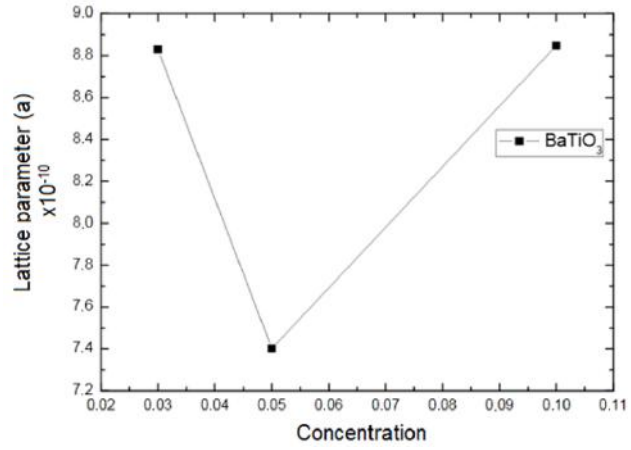

Fig. 14: Lattice Parameter "c" – Hexagonal Symmetry - calcined at 1200ºC.

From the results of the lattice parameters it was possible to notice an inverse increase in relation to the parameter "a" and "c" in the tetragonal symmetry, causing an increase in the c/a ratio, which is a favorable characteristic for the piezoelectric and ferroelectric properties. The change of lattice parameters occurs due to the substitution of Mn at the site occupied by Ti. Also, through the diffractograms and equations presented in this work, it was possible to calculate the theoretical densities of $BaTi_{(1-x)}Mn_xO_3$ samples for their respective concentrations. Results are presented in Table 2 and Figures 15 and 16.

Table 2 - Theoretical densities of calcined powders at 1200ºC of $BaTi_{(1-x)}Mn_xO_3$.

Substitution Dosage - Manganese	Phase	Theoretical density (g/cm³)
X=0.001	Tetragonal	5.9945
X=0.01	Tetragonal	6.0191
X=0.03	Tetragonal	6.0178
	Hexagonal	2.4967
X=0.05	Tetragonal	6.0337
	Hexagonal	2.4899
X=0.1	Hexagonal	2.5056

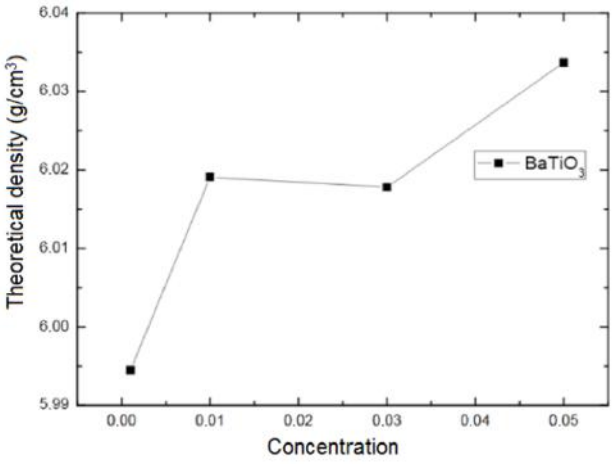

Fig. 15: Density relative to Mn dosage, Tetragonal phase.

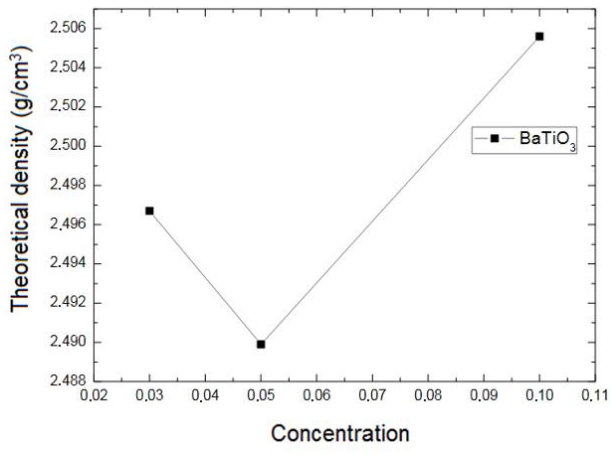

Fig. 16: Density relative to Mn dosage, Hexagonal phase.

The sample densities were measured for each concentration and since the powder from which of the samples were calcined at 1200 ºC, the theoretical density was 5.98402g/cm³ for the tetragonal structure and 2.4974g/cm³ for the hexagonal phase.

https://dx.doi.org/10.22161/ijaers.69.12 *ISSN: 2349-6495(P) | 2456-1908(O)*

Another result obtained in this work was the determination of the magnetic hysteresis curve in order to identify the presence of magnetism in the samples. The materials that presented such properties were those with concentration of 5% and 10% of Mn, with the highest magnetization value obtained for an applied magnetic field of 15000 Oe, the sample with the highest Mn concentration, ie x = 0.1, was ~ 0.05 emu / g, while for the sample of x = 0.05 the magnetization obtained was ~ 0.03 emu/g. For concentrations below 5% (x = 0.05) the results are not shown as the equipment was unable to measure.

As shown in Figure 17, the material analysis for x=0.05 showed low magnetization, not reaching saturation. The magnetic hysteresis curve shows an increase in magnetization as the applied field increases, generating for the highest applied field intensity 15000 Oe, the magnetization of ~ 0.03 emu/g, high values when compared to the literature. Rani et. al. (2015) was obtained for a 5000 Oe field, a magnetization of 0.006 emu / g, while in the present work, for an applied field of 5000 Oe, a magnetization of ~ 0.01 emu/g was obtained. The remaining magnetization for $BaTi_{(1-x)}Mn_xO_3$ with x=0.05 has values around 0.0006 emu/g. At 10% Mn concentration (x = 0.1), the remaining magnetization of $BaTi_{(1-x)}Mn_xO_3$ material has a higher value when compared to the 5% Mn concentration (x = 0.05) giving a value of ~ 0.001 emu/g.

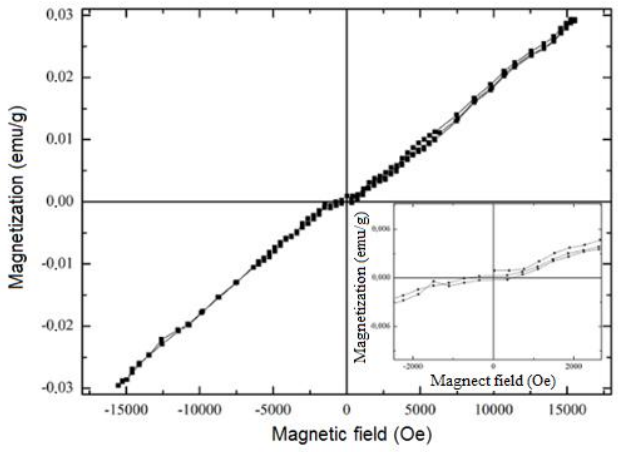

Fig. 17: Magnetic hysteresis measurements: $BaTi_{(1-x)}Mn_xO_3$ for the concentration of x=0.05

Figure 18 presents the analysis results for concentration of x = 0.1. In this material magnetization presents a better result than when compared to the lower Mn concentration material. For this material, the magnetization has a value of ~ 0.05 emu/g for an applied field of 15000 Oe. Rani et. al. (2015) presented for this same concentration and for an applied field of 5000 Oe a magnetization value of ~ 0.017 emu/g, while for this same field and concentration, the value obtained was ~ 0.019 emu/g.

The tetragonal to hexagonal phase transformation of the $BaTiO_3$ has been reported at high temperatures leading to high oxygen deficiency. Another considerable factor for the increase in oxygen vacancies is the increase in Mn concentration, having a greater amount of deficiency with a higher Mn concentration. Low substitution in $BaTi_{(1-x)}Mn_xO_3$ ceramics, oxygen vacancies are not high enough for complete transition from tetragonal to hexagonal phase. Induction of magnetism in $BaTi_{(1-x)}Mn_xO_3$ ceramics occurs due to the formation of oxygen vacancies and exchange interactions between different oxidation states of Mn [15]. Rani et. al. (2015) also state that the ferromagnetic order (FM) gradually increases with increasing concentration of ions Mn and with the change of oxidation state.

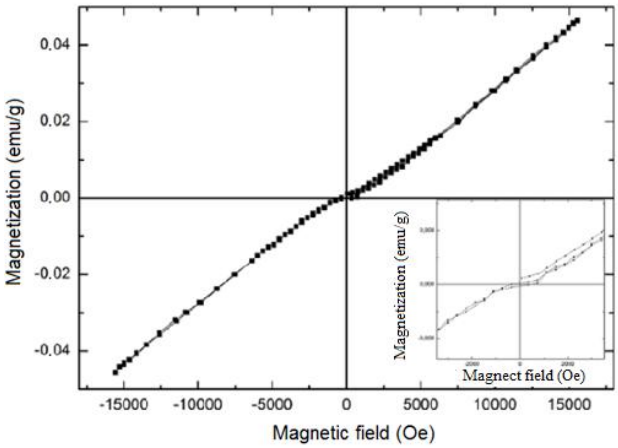

Fig. 18: Magnetic hysteresis measurements: $BaTi_{(1-x)}Mn_xO_3$ for the concentration of x = 0.1.

In the analyzes performed it was possible to verify low values for remaining magnetization, and it can be verified through magnetic hysteresis that there was a significant improvement in the remaining magnetization values with the increase of Mn concentration.

IV. CONCLUSION

Through the analyses of the diffractograms, it was possible to identify a change in the lattice parameters "a" and "c". Analyzing the samples that showed tetragonal symmetry, it was observed that as the concentration of the replacement ion Mn increased, the lattice parameter "c" increased, while the parameter "a" decreased. In order to explain the alteration of the lattice parameters, the influence of the concentration of the Mn dopant with different oxidation states should be taken into account, being incorporated into the $BaTiO_3$ tetragonal and hexagonal systems.

https://dx.doi.org/10.22161/ijaers.69.12 *ISSN: 2349-6495(P) | 2456-1908(O)*

As the concentration of Mn increases, cell stretching occurs, influencing the transformation of tetragonal to hexagonal symmetry. The incorporation of Mn ions into $BaTiO_3$ tetragonal cells causes crystal structure disorder, so the variation of $Mn^{(+3)}$, $Mn^{(+4)}$ ions concentration in the tetragonal and hexagonal structure are responsible for these changes in the lattice parameters.

The substitution of the Mn ions occurs at the Ti site and is responsible for the variations of the lattice parameters. The interaction between different oxidation states of Mn may reduce or increase size depending on the ion to be replaced. When this substitution occurs between the ions of $Mn^{(+3)}$ and $Ti^{(+4)}$ the lattice parameters increase, while when the substitution is made by a smaller ionic radius, that is, $Mn^{(+4)}$ occurs reduction of lattice parameters. Thus, it is concluded that $Mn^{(+3)}$ is located in the tetragonal symmetry, because with the increase of $Mn^{(+3)}$ concentration, the increase of "c" occurs. While $Mn^{(+4)}$ is located in hexagonal symmetry, thus parameter "a" decreases with increasing doping concentration. Making sure that when Mn assumes the position of Ti, the cell stretches as the concentration increases.

The phase structural transition, parameter variation, temperature, particle size, impurities and defect density directly influence the properties of $BaTi_{(1-x)}Mn_xO_3$. The properties of the material are also completely dependent on the concentration of Mn, increasing the concentration of the substituent ion is also responsible for the change in grain size. As the concentration of Mn increases, the material grains become coupled and reduce in size. Noting that the micro-structural growth habit and its distributions are completely dependent on Mn concentrations, and the grain size is responsible for the mechanical properties of a polycrystalline material.

The substitution of Mn ions by Ti ions in $BaTiO_3$ generated magnetic properties, and through the magnetic hysteresis curve it was possible to identify that with increasing manganese concentration the magnetization intensity also increased. For materials with a small percentage of Mn substitution, it was not possible to obtain magnetic measurements, as they presented low magnetization.

A magnetoelectric multiferroic material originated, as it presented ferroelectric and magnetic properties with increasing doping ion concentration, which can generate applications where the same material can perform more than one task and thus generate a growing interest in these materials.

ACKNOWLEDGEMENTS

This work was supported by FAESO (Faculdade Estácio de Sá de Ourinhos), Complexo de Centrais de Apoio à Pesquisa (Comcap) and Grupo de Desenvolvimento de dispositivos Multiferróicos (GDDM) of Universidade Estadual de Maringá.

REFERENCES

[1] Pereira, R. A. (2004). Synthesis and characterization of lanthanum and manganese doped hydrothermal barium titanate. 2004. 91 p. Master Thesis in Materials Engineering - REDEMAT, Federal University of Ouro Preto, Ouro Preto: School of Mines.

[2] Favarim, H.G.(2007). Synthesis, electrical and structural characterization of ferroelectric ceramics of $Ba0,90R0,10Ti_{1-x}Zr_xO_3$ composition (R = Ca, Sr). Thesis (Doctorate in Sciences) - São Carlos Institute of Physics, University of São Paulo, São Carlos, 2010Myers, D. G. Psychology(1stCanadian ed.). New York, NY: Worth.

[3] Tang, B., Zhang, S. R., Yuan, Y., Yang, L. B., & Zhou, X. H. (2007). Influence of tetragonality and secondary phase on the Curie temperature for barium titanate ceramics. Mater electron, v. 19, p.1109-1113. Novembro.

[4] Cerconi, C. (2012). Thermal and structural characterization of $BaTiO_3$ powders and thin films synthesized via Pechini method. 80 p. Master's Dissertation in Applied Chemistry - Midwestern State University, Guarapuava.

[5] Filho, M. A. A., Pinto, L. C. B. D. M., Oliveira, C. P. D., & Araujo, F. G. D. S. (2002). Influence of synthesis and firing temperatures on the sintering of hydrothermally obtained barium titanate ceramics. Rem: School of Mines Magazine, 55 (2), 89-92.

[6] Nanni, P.; Viviani, M.; Buscaglia, V. (1999). Synthesis of dielectric ceramic materials. Handbook of Low and High Dielectric Constant Materials and Their Applications. V. 1. San Diego, p. 429–455.

[7] Antonelli, E.; Bernardi, M. I. B.; Hernandes, A. C. (2005). $BaZr_3$ nanometric powders: preparation and characterization of ceramics. Ceramics, v. 51, p. 428-433.

[8] Brito, S. L. M.; Gouvêa, D. (2010). Surface characterization of $BaTiO_3$ nanoparticles prepared by the polymeric precursor method. Ceramic, v. 56 p. 228-236.

[9] Andrade, M. C., Assis, J. T., Pereira, F. R., Araujo, J. C., Moreira, E. L., Moraes, V. C. A., & Lopes, A. R. (2009). Characterization Of Barium Titanate Powder Doped With Sodium And Potassium Ions With Rietveld Refinement. Rio de Janeiro State University. Rio de Janeiro.

[10] Alves, M. F. S. (2012). Nanostructured Ceramics $BaTiO_3$: Synthesis And Structural And Ferrous Properties. 106 f. Master's dissertation in Physics - Maringá State University, Maringá.

[11] Oladeinde, T. O. (2010). Synthesis and electrical properties of doped barium titanate based ceramics Er_{3+} e Zr_{2+}: $Ba_{1-x}Er_x$ (Ti0,98Zr0,02)O3 (x= 0,01, 0,02, 0,04). 78 f. Final Paper in Electrical Engineering - University of São Paulo, São Carlos.

[12] Shuai, Y., Zhou, S., Bürger, D., Reuther, H., Skorupa, I., John, V., Schmidt, H. (2011). Decisive role of oxygen vacancy in ferroelectric versus ferromagnetic Mn-doped

https://dx.doi.org/10.22161/ijaers.69.12 *ISSN: 2349-6495(P) | 2456-1908(O)*

$BaTiO_3$ thin films. Journal of Applied Physics, 109(8), 084105.

[13] Lee, J. S., Khim, Z. G., Park, Y. D., Norton, D. P., Theodoropoulou, N. A., Hebard, A. F., ... & Wilson, R. G. (2003). Magnetic properties of Co-and Mn-implanted $BaTiO_3$, $SrTiO_3$ and $KTaO_3$. Solid-State Electronics, 47(12), 2225-2230.

[14] Padilha, A. F. (2000). Engineering Materials: Microstructure and Properties. 1 ed. Curitiba: Hemus publisher S.A.

[15] Rani, A. Kolte, J. Gopalan, P. (2015). Phase formation, microstructure, electrical and magnetic properties of Mn substituted barium titanate. Ceramics International.

[16] Callister, W. D., & Rethwisch, D. G. (2007). Materials science and engineering: an introduction (Vol. 7, pp. 665-715). New York: John wiley & sons.

[17] Dias, Larissa G. (2017). Preparation, Structural And Magnetic Characterization Of The $Bati_{(1-X)}Mn_xo_3$ System. 60f. Master Thesis in Mechanical Engineering - Federal Technological University of Paraná. Cornélio Procópio, Paraná, Brasil.